Targeting AXL Inhibits the Growth and Metastasis of Prostate Cancer in Bone

Chun-Lung Chiu[1], Dalin Zhang[1], Hongjuan Zhao[1], Yi Wei[1], Alexandra Lapat Polasko[1], Mikkel Thy Thomsen[1,2], Vanessa Yang[1], Kasie Kexin Yang[1], Spencer Hauck[3], Eric E. Peterson[1], Ru M. Wen[1], Zhengyuan Qiu[1], Eva Corey[4], Yu Rebecca Miao[5], Erinn B. Rankin[5], Donna M. Peehl[6], Jiaoti Huang[3], Amato J. Giaccia[5,7], and James D. Brooks[1,8]

ABSTRACT

Purpose: After failing primary and secondary hormonal therapy, castration-resistant and neuroendocrine prostate cancer metastatic to the bone is invariably lethal, although treatment with docetaxel and carboplatin can modestly improve survival. Therefore, agents targeting biologically relevant pathways in prostate cancer and potentially synergizing with docetaxel and carboplatin in inhibiting bone metastasis growth are urgently needed.

Experimental Design: Phosphorylated (activated) AXL expression in human prostate cancer bone metastases was assessed by IHC staining. We evaluated the effects of a novel soluble AXL signaling inhibitor, sAXL (batiraxcept or AVB-S6-500), on tumor growth and lung metastases in prostate cancer patient-derived xenograft models that were implanted intratibially. After injection of LuCaP cells into the tibiae, tumors were treated with batiraxcept and docetaxel or carboplatin alone or in combination, and tumor growth was monitored by serum prostate-specific antigen or bioluminescence. Tumor burden was quantified by human-specific Ku70 staining, and metastasis to the lungs was determined using qPCR. Transcriptomic profiling, Western blotting, and immunohistochemistry were performed to identify treatment-regulated gene and protein profile changes.

Results: High AXL phosphorylation in human prostate cancer bone metastases correlated with shortened survival. Batiraxcept alone or in combination with docetaxel or carboplatin significantly suppressed intratibial tumor growth and suppressed metastasis to the lungs through multiple mechanisms, including repression of cancer stemness genes (*CD44*, *ALDH1A1*, *TACSTD2*, and *ATXN1*) and the PI3K, JAK, MAPK, and E2F1/NUSAP1 signaling pathways.

Conclusions: Our study provides a robust preclinical rationale and mechanisms of action for using batiraxcept as a single agent or in combination with docetaxel or carboplatin to treat lethal metastatic prostate cancer.

Introduction

An estimated 35,250 patients with prostate cancer will succumb to the disease in the United States in 2024, and the 5-year overall survival (OS) rate in metastatic prostate cancer (mPCa) is ≤34% (1). In advanced prostate cancer, bone metastasis occurs commonly (2) and produces considerable morbidity due to fractures, intolerable bone pain, and spinal cord compression (3). Androgen deprivation therapy (ADT) has been the standard of care for high-risk non-metastatic prostate cancer and metastatic hormone-sensitive prostate cancer (4). Although nearly all prostate cancers respond to ADT, nearly all patients progress to metastatic castration-resistant adenocarcinoma (mCRPC AC) within months to years (5), for which the median OS time is <2 years (2, 6). Treatment of mCRPC AC with second-generation antiandrogens such as abiraterone and enzalutamide frequently induces transdifferentiation of adenocarcinomas to the more aggressive and lethal variant neuroendocrine prostate cancer (NEPC; ref. 7). In addition, responses to docetaxel as the first-line chemotherapy for mCRPC AC and platinum-based therapy such as carboplatin for NEPC are short-lived, and resistance occurs quickly (8). Moreover, the efficacy of FDA-approved bone-targeting therapies for mCRPC, such as bisphosphonates, denosumab, radium-223, and Lutetium-177 PSMA, is limited (9). Therefore, effective bone metastasis–targeting therapies for mCRPC patients are urgently needed.

Dysregulation of the AXL signaling pathway can enhance tumor growth and metastasis (10). In prostate cancer, AXL signaling has been shown to drive tumor growth (11), progression (12), bone metastasis (13), resistance to docetaxel (14), and ADT (15). AXL is overexpressed in primary prostate cancer and mPCa tissues compared with non-cancerous prostate tissues (11, 16) and correlates with tumor grade (16). Genetic inhibition of AXL in prostate cancer cells significantly prolonged OS in a preclinical intracardiac injection model (17), supporting the importance of AXL in disease progression. Notably, a recent study revealed that AXL signaling is a key driver of the CRPC-stem cell–like (CRPC-SCL) subtype, which is less responsive to ADT (18). In the bone marrow niche, AXL signaling promotes prostate cancer invasion, proliferation, survival (16, 19), and establishment of PCa stem cells (CSC; ref. 20). Therefore, AXL signaling is a potential therapeutic target for bone metastases in mPCa (21).

[1]Department of Urology, Stanford University School of Medicine, Stanford, California. [2]Department of Clinical Medicine, Aarhus University, Aarhus Centrum, Denmark. [3]Department of Pathology, Duke University School of Medicine, Durham, North Carolina. [4]Department of Urology, University of Washington, Seattle, Washington. [5]Department of Radiation Oncology, Stanford University School of Medicine, Stanford, California. [6]Department of Radiology and Biomedical Imaging, University of California, San Francisco, San Francisco, California. [7]Department of Oncology, University of Oxford, Oxford, United Kingdom. [8]Stanford Cancer Research Institute, Stanford University School of Medicine, Stanford, California.

C.-L. Chiu and D. Zhang contributed equally to this article.

Corresponding Author: James D. Brooks, Department of Urology, Stanford University School of Medicine, Stanford, CA 94305. E-mail: jdbrooks@stanford.edu

Clin Cancer Res 2025;31:1346–58

doi: 10.1158/1078-0432.CCR-24-3028

Translational Relevance

We evaluated the efficacy of soluble AXL (sAXL or batiraxcept), a decoy receptor that can potently inhibit AXL signaling, as a single agent or in combination with docetaxel or carboplatin to treat prostate cancer bone metastases. We used intratibial injection of multiple patient-derived xenografts with different characteristics, reflecting a traditional phase II clinical trial without preselection for a particular tumor characteristic. Inhibition of tyrosine kinase receptor AXL was highly effective as a single agent and further reduced tumor growth when combined with docetaxel or carboplatin in suppressing prostate cancer tumor growth in the bone and metastasis to the lungs. AXL inhibition downregulated the expression of critical cancer stem cell–related genes, suppressed E2F1/NUSAP1 signaling pathways, and significantly decreased tumor growth and metastasis. Our findings provide compelling preclinical data for testing batiraxcept in patients with prostate cancer with bone metastases.

We investigated the clinical relevance of AXL protein phosphorylation, which activates AXL signaling, in bone specimens from mCRPC patients. We also evaluated the effects of batiraxcept (AVB-S6-500; ref. 22), a novel ultra–high-affinity soluble AXL (sAXL) decoy receptor capable of sequestering growth arrest–specific 6 (GAS6), the ligand of the AXL receptor, as a single agent or in combination with docetaxel or carboplatin, standard-of-care chemotherapeutic agents for mCRPC and NEPC, respectively, on bone tumor growth and lung metastases using intratibial patient-derived xenograft (PDX) models. Finally, we investigated the molecular mechanisms of action of batiraxcept by identification of treatment-regulated gene and protein profile changes.

Materials and Methods

Reagents

All antibodies used in this study are listed in Supplementary Table S1.

Cell culture

LuCaP 147, 147CR, 35 (RRID:CVCL_4853), and 35CR xenografts were obtained from the Department of Urology, University of Washington, and spheroids were generated and cultured in StemPro hESC SFM (Invitrogen) supplemented with 10 nmol/L of R1881 and 2 μmol/L of Y-27632, as described previously (23, 24), and incubated at 37°C with 5% CO_2. The LuCaP spheroids were tested by short-tandem repeat analysis and proved to be unique and of human male origin (23), and mycoplasma testing was conducted routinely.

Generation of luciferase-expressing LuCaP 49 spheroids

The stable LuCaP 49 (RRID:CVCL_4750) luciferase-expressing cells (LuCaP 49-luc) were generated with a pLenti CMV V5-LUC Blast vector (RRID:Addgene_21474) and selected in StemPro hESC SFM containing 2 μg/mL blasticidin as described (25). The dual-luciferase reporter assay system (Promega) was used to confirm the luciferase expression.

Patient tumor specimens and IHC staining

Human prostate cancer bone biopsy specimens were obtained from the Stand Up 2 Cancer/Prostate Cancer Foundation–funded West Coast Prostate Cancer Dream Team project under an approved protocol overseen by the UCSF Institutional Review Board and conducted in accordance with the Belmont Report implemented through the Common Rule. All individuals provided written informed consent (7, 26).

The formalin-fixed and paraffin-embedded specimens ($n = 31$) were used to perform IHC staining using anti–phospho-AXL, as described previously (25, 27, 28), using a protocol supplied by the manufacturer (Cell Signaling). Immunostaining was carried out using the VECTASTAIN ABC system, according to the manufacturer's instructions (Vector Laboratories). A four-point staining intensity scoring system was applied by two independent pathologists to quantify the relative expression of phospho-AXL in cancer components of the specimens (29, 30).

Animal studies

All procedures complied with the Stanford University Institutional Animal Care and Use Committee and NIH guidelines. LuCaP 147, 147CR, 35, 35CR, 49, or LuCaP 49-luc spheroids were cultured in ultralow attachment plates (Corning; ref. 25). Variable responses to therapeutic agents in LuCaP PDXs have been reported (31). Assuming the variation in tumor growth among mice carrying the same LuCaP PDX line is 20%, nine mice per group were estimated to be necessary to detect a 35% inhibition in tumor growth with 80% power and an alpha value of 0.05.

Spheroids were dissociated enzymatically with ACCUTASE (Invitrogen) and mechanically using a fire-polished Pasteur pipette. The cell mixture was passed through a 40-μm sieve, and disaggregation into single cells was confirmed microscopically. HEPES-buffered saline (HBS; 20 μL) containing 2×10^5 single cells was injected into the right tibiae of 6- to 8-week-old male $RAG2^{-/-}\gamma C^{-/-}$ mice, as described previously (25). For LuCaP 35CR and 147CR lines, androgen deprivation was accomplished by surgical castration of the mice. Serum prostate-specific antigen (PSA) levels were determined in mice bearing LuCaP 147, 147CR, 35, and 35CR at days 14 and 28 using a human PSA-total ELISA kit (Sigma-Aldrich) according to the manufacturer's instructions. Mice were randomized into four groups, and the levels of murine serum GAS6 were determined for all treatment groups for the LuCaP 147 PDXs before treatment initiation using a mouse GAS6 ELISA kit (Sigma-Aldrich). All groups were treated for 30 days by intraperitoneal injection: phosphate-buffered saline (Vehicle), batiraxcept [20 mg/kg/every other day (QOD)], docetaxel [10 mg/kg/once a week (QW)], and batiraxcept (20 mg/kg/QOD) + docetaxel (10 mg/kg/QW). LuCaP 49–luc cell growth was monitored by whole-body bioluminescence intensity (BLI) imaging using a Lago optical imaging system (Bruker) on days 14 and 28. Mice were then randomized into four groups for 30 days of treatment by intraperitoneal injection: phosphate-buffered saline (Vehicle), batiraxcept (20 mg/kg/QOD), carboplatin (5 mg/kg/QW), and batiraxcept (20 mg/kg/QOD) + carboplatin (5 mg/kg/QW). MicroCT was performed using a Bruker Skyscan 1276 (Bruker) at the Stanford Center for Innovation in *In Vivo* Imaging. Image analysis and 3D representations were conducted with GEHC Micro View Version MicroView Analysis (GE HealthCare). After sacrifice, the tumor-bearing legs and organs were harvested. The contralateral hind legs of the animals were harvested as controls for histomorphometric analysis.

Mouse specimens and quantification of IHC signals

Intratibial PDX and lung lobes were fixed in 10% buffered formalin overnight (25). Mice tibiae were fixed in 10% buffered formalin for 2 days and incubated in 14% ethylenediamine tetraacetic acid (EDTA; Sigma-Aldrich) to decalcify for 15 days. After embedding in paraffin, 5-μm slices were sectioned for Masson–Goldner staining and IHC using a human Ku70 antibody to evaluate the treatment response (32, 33). IHC for lung lobes and tibiae of mice was performed as described previously (25, 27, 29, 30, 34). The IHC signals from murine tibial sections were analyzed and quantified by ImageJ software version 1.54f as described (34). We used one slide from a matching area of every mouse tibia in each treatment arm (8–9 mice per arm). Therefore, 32 to 36 slides were used for each LuCaP PDX line for Ku70 quantification.

Immunofluorescence

Mouse tibial sections were deparaffinized and rehydrated before antigen retrieval (0.1% trypsin for 5 minutes), followed by incubation with blocking serum and appropriate antibodies overnight at 4°C, followed by 1-hour incubation with secondary antibodies, Alexa 488 (Abcam Cat. # ab150113, RRID:AB_2576208, Abcam Cat. # ab150077, RRID:AB_2630356) or Alexa 555 (Thermo Fisher Scientific Cat. # A-21422, RRID:AB_2535844), at room temperature. Slides were mounted with DAPI Fluoromount-G (DAPI, or 4′,6 diamidino-2-phenylindole; Southern Biotech) and imaged using Leica Application Suite X software on a Leica CTR 6500 (Leica; ref. 35).

RNA extraction and qRT-PCR

Total RNA from mouse tissues was purified using the Qiagen RNeasy Mini Kit (Qiagen) and subject to DNase treatment using the RNase-Free DNase Set (Qiagen) or TURBO DNA-free Kit (Life Technologies). Relative gene expression was determined by qRT-PCR with the ΔCT method using human-specific GAPDH (forward: 5′-AGATCCCTCCAAAATCAAGTG-3′; reverse: 5′-CAAAGTTGTCATGGATGACC-3′) and universal GAPDH (forward: 5′-CCATGGAGAAGGCTGGGG-3′; reverse: 5′-CAAAGTTGTCATGGATGACC-3′) reference genes (36).

RNA-seq and expression analysis

RNA-seq was performed by Novogene using the Illumina NovaSeq PE150 platform, a paired-end sequencing technology with a 150 bp read length (37). We aligned the reads to both human and mouse genomes (hg38 and mm10), imported these aligned files into R, and used the R package "XenofilteR" v. 1.6 to remove all mouse reads from the dataset. The reference genome and gene model annotation files were downloaded from the genome website directly. Hisat2 v2.0.5 was used to build the index of the reference genome, and paired-end clean reads were aligned to the reference genome. The read numbers mapped to each gene were counted by featureCounts v1.5.0-p3. The FPKM value of each gene was determined by the length of the gene and read counts mapped to the gene. Raw data are available at Gene Expression Omnibus (GSE281461). Differential expression analysis of two conditions (with two biological replicates per condition) was conducted using the DESeq2 R package (version 1.20.0). Adjusted *P*-values were obtained using Benjamini and Hochberg's method to control the false discovery rate. Genes with an adjusted *P*-value ≤ 0.05, as determined by DESeq2, were designated as differentially expressed. Additionally, gene set enrichment analysis (GSEA) was performed using GSEA version 3.0. Adjusted *P*-values <0.05 and FDR < 0.25 were considered statistically significant. Heatmaps were generated using genes from the GSEA software, with batiraxcept versus vehicle gene expression as the phenotype label.

Protein extraction and Western blots

Protein extraction and Western blots were performed as described previously (34, 35). Blot visualization was achieved using SuperSignal West Femto Maximum Sensitivity Substrate (Thermo Fisher Scientific), Amersham ECL Western Blotting Detection Reagent (GE HealthCare), or Clarity ECL Western Blotting Substrate (Bio-Rad), followed by imaging using Image Lab software on a ChemiDoc XRS System (Bio-Rad).

Statistical analysis

Univariable and multivariable Cox proportional hazards models were utilized to assess whether p-AXL IHC staining was associated with survival time, without and with adjustments of ECOG scores, PSA, LDH, ALP, and hemoglobin levels at the time of biopsy. *P*-values < 0.05 were considered statistically significant. For the Kaplan–Meier analysis, the log-rank test was performed to assess significance. These analyses were performed using SAS statistical software (version 9.34, SAS Institute). Additional statistical analyses were performed using GraphPad Prism 10.2.3 (GraphPad Software). A one-way ANOVA test followed by Tukey's test was used to correct the multiple comparisons. An unpaired *t* test (parametric) or two-tailed Mann–Whitney test (nonparametric) was used for pairwise comparison. All error bars represent the mean ± SEM. Notably, *P*-values are indicated as *, $P < 0.05$; **, $P < 0.01$; ***, $P < 0.001$; NS, $P > 0.05$ not significant.

Data availability

RNA sequencing (RNA-seq) data from LuCaP PDX xenografts are available at Gene Expression Omnibus (GSE281461). Other raw data in this study are available upon request to the corresponding author.

Results

High AXL phosphorylation correlated with poor clinical outcomes in patients with mCRPC

To determine the correlation of phosphorylated AXL (p-AXL) protein levels with clinical outcomes in human bone metastases, we evaluated the p-AXL expression in 31 mCRPC bone biopsies by IHC using a 4-point IHC scoring system (Supplementary Table S2; ref. 29). Twelve patients showed low p-AXL expression with staining observed in 0% to 1% of the cells (staining intensity score = 0; **Fig. 1A**) or in less than 10% of the cells (staining intensity score = +1; **Fig. 1B**), whereas 19 patients showed high p-AXL expression with staining present in 10%–50% of the cells (staining intensity score = +2; **Fig. 1C**) or more than 50% of the cells (staining intensity score = +3; **Fig. 1D**). Kaplan–Meier analysis revealed an inverse correlation of p-AXL protein expression levels in bone metastases with OS in this patient cohort (**Fig. 1E**). Both univariable and multivariable logistic regression analyses (**Fig. 1F**) showed that high p-AXL protein expression was significantly associated with survival outcomes. Overall, these results indicate that high p-AXL protein expression in bone metastases is associated with shortened survival in patients with mCRPC.

Batiraxcept as a single agent or in combination with docetaxel significantly inhibited growth and metastasis of LuCaP mPCa AC PDX in bone tissues

To evaluate the effects of AXL inhibition in the bone microenvironment, we administered the sAXL receptor, batiraxcept (AVB-S6-500),

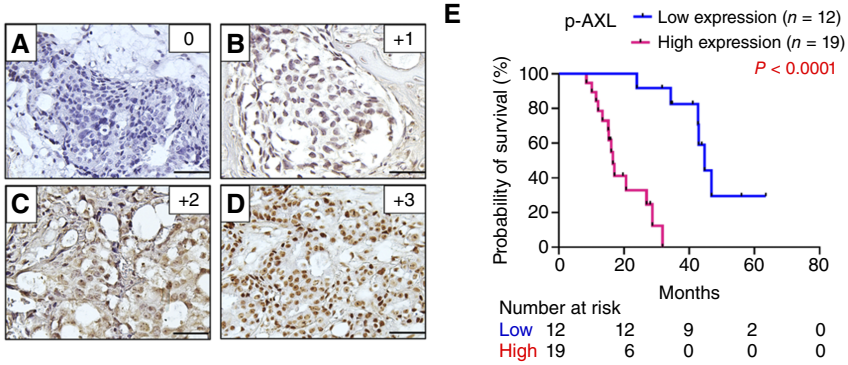

Figure 1.

High p-AXL level is correlated with shorter survival in mCRPC. **A–D,** Representative images of p-AXL expression in mCRPC bone metastases by IHC. Scale bars, 50 μm. Negative staining (**A**, score = 0). Weak staining (**B**, score = +1). Moderate staining (**C**, score = +2). Intense staining (**D**, score = +3). **E,** Kaplan–Meier analysis of patients with mCRPC with low and high p-AXL expression in bone metastases. Log-rank (Mantel–Cox) test, $P < 0.0001$. **F,** Univariable and multivariable regression analyses of p-AXL, ECOG PS, PSA, LDH, ALP, and hemoglobin predictive of survival outcomes. ECOG PS: Eastern Cooperative Oncology Group Performance Status. PSA, LDH, and hemoglobin were detected at biopsy.

F

Variable	*N* (%) or mean ± STD		Univariable		Multivariable	
			Crude HR (95% CI)	*P* value	aHR (95% CI)	*P* value
p-AXL						
Low	12 (38.7)	High vs. low	ref		ref	
High	19 (61.3)		29.3 (3.61–237.7)	0.002	26.9 (3.03–238.4)	0.003
ECOG PS						
0	23 (74.2)		ref	0.17	ref	
1	7 (22.6)	1 vs. 0	1.53 (0.52–4.47)	0.43	0.96 (0.28–3.27)	0.95
2	1 (3.2)	2 vs. 0	7.80 (0.85–72.1)	0.07	2.84 (0.18–45.7)	0.46
PSA	145.9 ± 260.5		1.004 (1.002–1.006)	0.0004	1.003 (0.999–1.01)	0.12
LDH	220.9 ± 77.0		1.01 (1.001–1.02)	0.03	0.999 (0.99–1.01)	0.84
ALP	220.9 ± 233.1		1.003 (1.001–1.004)	0.003	1.00 (0.997–1.003)	0.96
Hemoglobin	12.9 ± 1.6		0.59 (0.44–0.79)	0.0004	0.73 (0.48–1.10)	0.14

that sequesters the AXL ligand GAS6 (**Fig. 2A**), either alone or in combination with docetaxel or carboplatin, using an intratibial injection model of prostate cancer bone metastases (**Fig. 2B**). To represent the heterogeneity of mPCa, we implanted cells from five LuCaP PDXs, including four adenocarcinomas (AC), namely, LuCaP 35, 147, and their derived castration-resistant (CR) lines, 35CR and 147CR, and one NEPC, LuCaP 49. Analysis of previously published RNA-seq data (31) demonstrated that AXL mRNA levels were similar in LuCaP 35, 35CR, 147, and 49 (**Fig. 2C**), whereas GAS6 levels were higher in 35 and 35CR than in 147 and 49 (**Fig. 2D**). In addition, 35/35CR and 147/147CR have been shown previously to display differences in serum PSA levels and in responsiveness to docetaxel (**Fig. 2E**; ref. 31). Therefore, LuCaP 35, 35CR, 147, 147CR, and 49 appeared to be appropriate PDX models to evaluate the treatment effects of batiraxcept, docetaxel/carboplatin, and batiraxcept + docetaxel/carboplatin combination therapy.

A previous study (38) had demonstrated that murine GAS6 can regulate the proliferation of human PC3 cells. We, therefore, measured levels of mouse serum GAS6 in all arms of the LuCAP147 mice before treatment by ELISA and found no significant differences in murine serum GAS6 levels between groups (Supplementary Fig. S1). The growth of tumors in bone was evaluated by IHC staining for human-specific Ku70 antigen (**Fig. 3A** and **B**; Supplementary Fig. S2A and S2B), as described previously (25, 32, 33). Both batiraxcept and docetaxel as single agents significantly reduced the growth of all four LuCaP mPCa AC PDX (**Fig. 3C** and **D**; Supplementary Fig. S2C and S2D). In addition, batiraxcept outperformed docetaxel in the two mCRPC AC PDX, 147CR and 35CR, but not in their hormone-sensitive counterparts, 147 and 35, suggesting batiraxcept was more effective than docetaxel in suppressing tumor growth of mCRPC AC in bone. Moreover, the combination of batiraxcept and docetaxel led to the greatest suppression (75%–95%) of tumor growth in the bone of all four mPCa AC PDX. Interestingly, 147CR and 35CR (**Fig. 3A** and **B**) were more resistant to docetaxel than 147 and 35 (Supplementary Fig. S2A and S2B) in the intratibial xenograft models, suggesting that progression to androgen independence promotes resistance to docetaxel in mPCa AC in the bone microenvironment. In contrast, 147CR and 35CR were more sensitive to batiraxcept than 147 and 35, indicating a greater dependency of androgen-independent mPCa AC on AXL signaling compared with their parental lines. Therefore, batiraxcept as a single agent appeared to be more effective than docetaxel, particularly for androgen-independent bone metastases. Furthermore, batiraxcept further inhibited tumor growth in bone when combined with docetaxel regardless of androgen dependency.

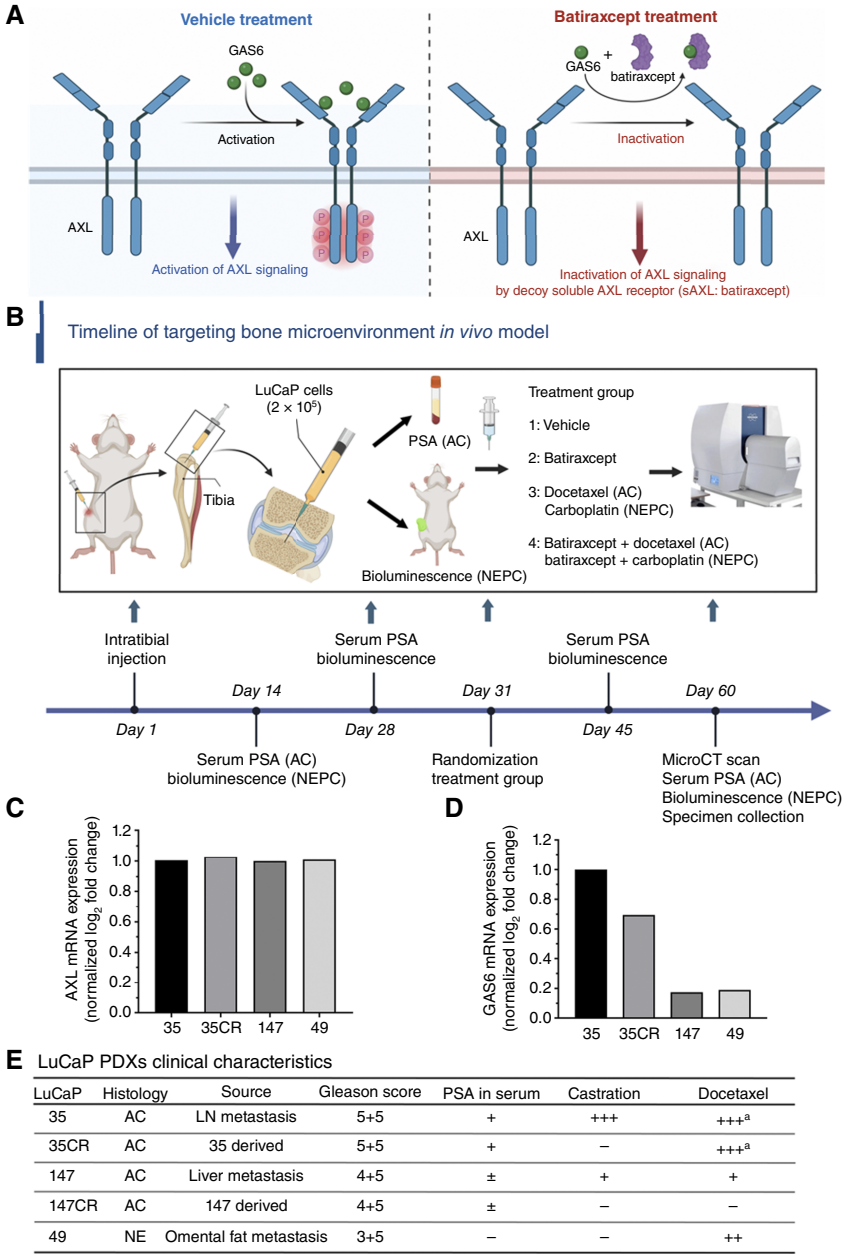

E LuCaP PDXs clinical characteristics

LuCaP	Histology	Source	Gleason score	PSA in serum	Castration	Docetaxel
35	AC	LN metastasis	5+5	+	+++	+++[a]
35CR	AC	35 derived	5+5	+	–	+++[a]
147	AC	Liver metastasis	4+5	±	+	+
147CR	AC	147 derived	4+5	±	–	–
49	NE	Omental fat metastasis	3+5	–	–	++

Figure 2.
Schematic diagram illustrating experimental design to evaluate AXL inhibition in the growth and metastasis of tumors in bone using prostate cancer PDX. **A,** Mechanism of action of the sAXL decoy receptor (batiraxcept/AVB-S6-500). **B,** Timeline of tumor generation in bone and treatments. **C** and **D,** AXL (**C**) and GAS6 (**D**) gene expression in LuCaP 35, 35CR, 147, and 49 PDX cell lines from GSE66187. **E,** Characteristics of LuCaP PDX used in this study (31). AC, adenocarcinoma; CR, castration-resistant; LN, lymph node. NE, neuroendocrine; PSA in serum, +, 5–100 ng/mL; ±, 0.1–4.9 ng/mL, –, not detected. Response to castration and docetaxel in the mouse subcutaneous xenograft model: +++, tumor volume decreases significantly for a prolonged period; ++, tumors progress but slower than control tumors; +, negligible response; –, no response; a, treatment increased body weight loss. (**A** and **B,** Created with BioRender. Chiu, C. [2025], https://BioRender.com/w55j627 and https://BioRender.com/r82y980.)

Batiraxcept and docetaxel as single agents or in combination reduced mouse serum PSA (Supplementary Fig S3) and increased bone mineral density of the tibiae to a similar extent, as determined by microCT (Supplementary Fig S4). None of the treatment groups displayed significant differences in body weight, indicating an overall low toxicity of batiraxcept, docetaxel, and combination therapy at the doses administered (Supplementary Fig S5).

In lung tissues from vehicle-treated mice carrying LuCaP 147CR and 35CR PDX intratibial tumors, we observed large Ku70- and AR-positive tumor nodules, whereas small clusters of tumor cells were found in docetaxel-treated mice (**Fig. 3E**; Supplementary Fig S2E). In contrast, Ku70-positive cells were rarely present in lung tissues from batiraxcept-treated mice, suggesting AXL inhibition significantly decreased metastasis from bone to the lungs. These tumor nodules/clusters were negative for neuroendocrine marker SYP, indicating that they were AC and not NEPC (**Fig. 3E**; Supplementary Fig S2E). To quantify the amount of prostate cancer cells in the lungs, we performed qRT-PCR using human-specific and universal GAPDH primers in LuCaP 147CR and 35CR PDX lung tissues. Consistent with IHC staining, the percentages of tumor cells were extremely low in lungs of batiraxcept-treated mice compared with vehicle-treated mice, whereas approximately one-fourth of metastatic tumor cells were observed in lungs of docetaxel-treated mice compared with the control (**Fig. 3F**; Supplementary Fig S2F), demonstrating that batiraxcept as a single agent or in combination with docetaxel can robustly inhibit CRPC metastasis from the mouse tibiae to the lungs.

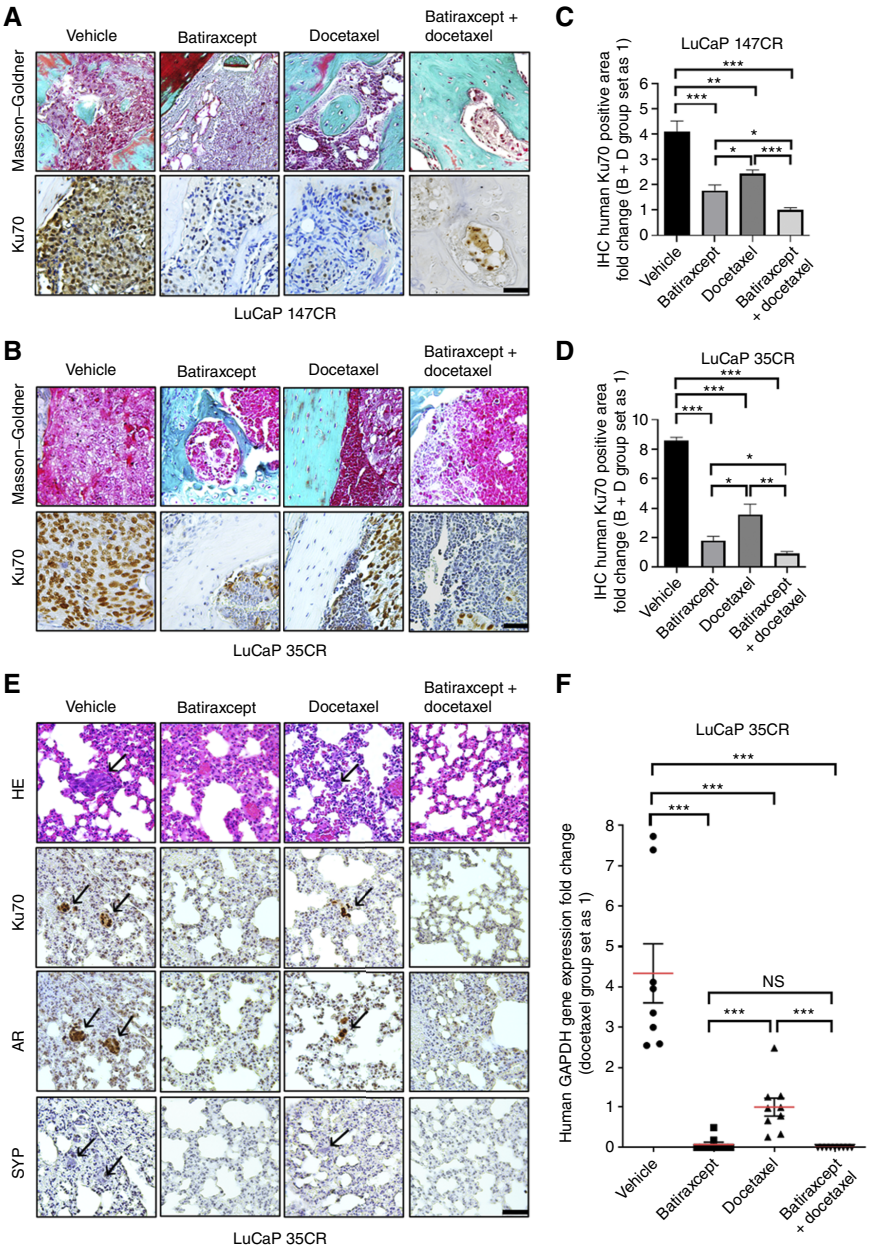

Figure 3.

Batiraxcept and docetaxel alone or in combination significantly inhibited bone tumor growth and metastasis in LuCaP mCRPCa AC PDX models. **A** and **B,** Representative images of Masson–Goldner staining and Ku70 IHC of PDX cells in the tibiae of LuCaP 147CR (**A**) and LuCaP 35CR (**B**). Human CRPCa cells marked by Ku70 were significantly decreased after 30 days of treatment by intraperitoneal injection with batiraxcept (20 mg/kg/QOD, $n = 8$–9), docetaxel (10 mg/kg/QW, $n = 9$), or the combination of batiraxcept (20 mg/kg/QOD, $n = 9$) and docetaxel (10 mg/kg/QW, $n = 9$) compared with vehicle controls ($n = 8$–9). **C** and **D,** Quantification of the IHC Ku70–positive areas in mouse tibia specimens treated with vehicle, batiraxcept, docetaxel, and batiraxcept + docetaxel in **A** and **B**. Fold change: combination batiraxcept and docetaxel (B + D) group set as 1. **E,** Inhibition of LuCaP 35CR tumor cells metastasis to mouse lung lobes by batiraxcept, docetaxel, and batiraxcept + docetaxel combination therapy. The arrowheads indicate Ku70-positive metastatic tumor nodules in the lungs, which metastasized from the mice tibiae. **F,** Quantification of fold changes (docetaxel group set as (i) of human-specific GAPDH level normalized against universal GAPDH level in different treatment groups for LuCaP 35CR. *, $P < 0.05$; **, $P < 0.01$; ***, $P < 0.001$; NS, $P > 0.05$ not significant. All scale bars, 50 μm.

Batiraxcept as a single agent or in combination with carboplatin significantly inhibited NEPC intratibial tumor growth and metastasis to the lungs

LuCaP 49 was derived from a patient with poorly differentiated NEPC (**Fig. 2E**). We generated stable luciferase-expressing cells by lentiviral transduction and implanted them intratibially. Bioluminescence was measured at 2 and 4 weeks after injection, and 35 mice were randomized into vehicle (PBS, $n = 8$), batiraxcept (20 mg/kg/QOD, $n = 9$), carboplatin (5 mg/kg/QW, $n = 9$), and combination therapy of batiraxcept (20 mg/kg/QOD, $n = 9$) and carboplatin (5 mg/kg/QW, $n = 9$; **Fig. 4A**) treatment groups. Batiraxcept as a single agent outperformed carboplatin in inhibiting intratibial tumor growth, as determined by bioluminescence imaging (**Fig. 4B**) and Ku70 IHC staining (**Fig. 4C** and **D**). Combination therapy significantly reduced tumor growth compared with carboplatin alone based on bioluminescence imaging. However, combination therapy compared with batiraxcept alone did not show statistically significant differences in suppression of tumor growth based on bioluminescence imaging (**Fig. 4A** and **B**). In contrast, analysis of tibiae by Ku70 IHC staining demonstrated that batiraxcept + carboplatin decreased tumor growth to a greater degree than batiraxcept alone and carboplatin alone (**Fig. 4C** and **D**). As observed in the LuCaP AC PDX models, batiraxcept outperformed carboplatin in inhibiting NEPC LuCaP 49 metastases to the lungs. Specifically, No Ku70- or SYP-positive tumor cells were observed in batiraxcept-treated compared with vehicle-treated tissues, while fewer Ku70- and SYP-positive tumor cell clusters were observed in carboplatin-treated tissues compared with vehicle-treated tissues. These cell

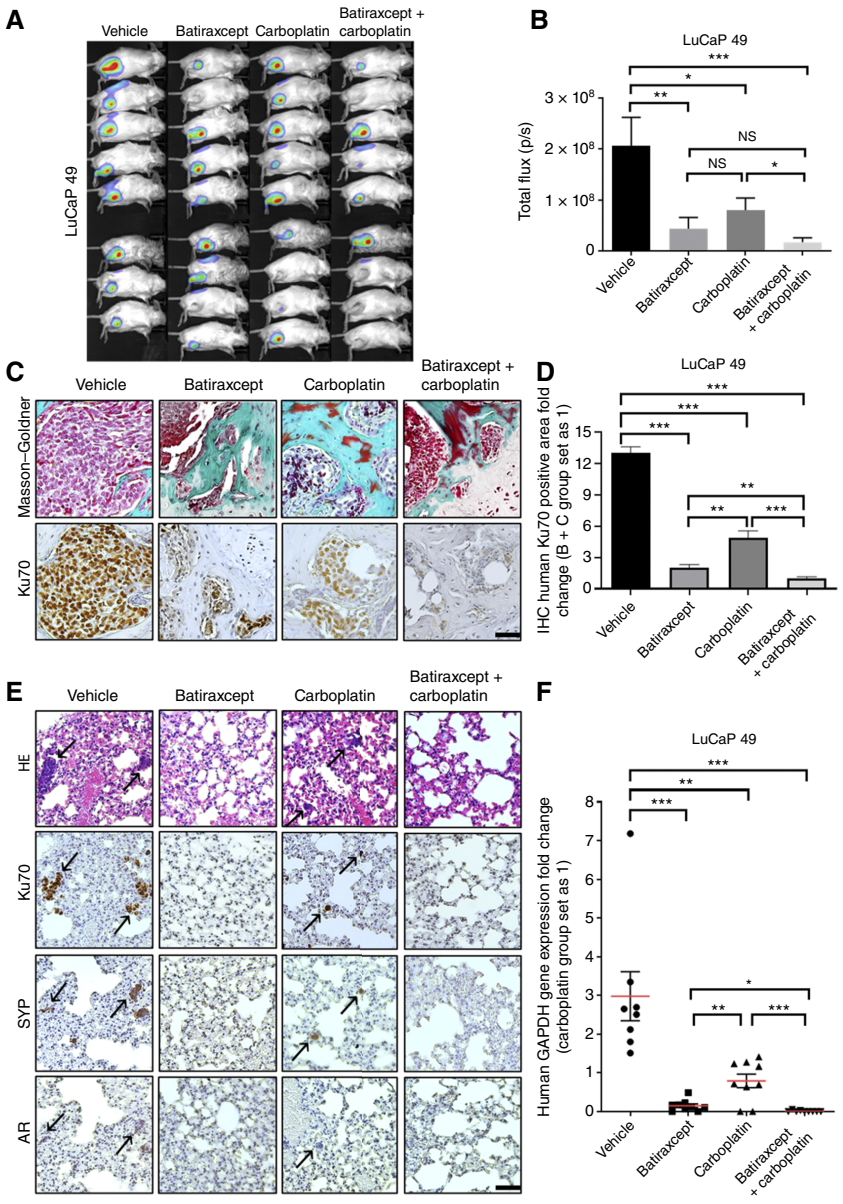

Figure 4.

Batiraxcept alone and in combination with carboplatin inhibited tumor growth and metastasis in the LuCaP 49 NEPC PDX model. Tumor-bearing mice ($n = 35$) were injected intraperitoneally for 30 days with vehicle (PBS, $n = 8$), batiraxcept (20 mg/kg/QOD, $n = 9$), carboplatin (5 mg/kg/QW, $n = 9$), or batiraxcept (20 mg/kg/QOD, $n = 9$) + carboplatin (5 mg/kg/QW, $n = 9$). **A,** Representative images of tumor bioluminescence. **B,** Quantification of whole-body bioluminescence on day 30 after intratibial injection of 1×10^5 luciferase-labeled LuCaP 49 cells into the right tibiae of male RAG2$^{-/-}\gamma C^{-/-}$ immunodeficient mice ($n = 8$–9 per arm). **C,** Ku70 expression of LuCaP 49 cells in mouse tibiae. **D,** Quantification of intratibial LuCaP 49 cells in control and treatment groups. **E,** Representative lung metastases (arrows) stained with anti-Ku70, SYP, and AR antibodies. **F,** Quantification of human-specific GAPDH fold-changes (carboplatin group set as 1) by qRT-PCR in mouse lungs from each of the treatment groups. *, $P < 0.05$; **, $P < 0.01$; ***, $P < 0.001$; NS, $P > 0.05$ not significant. All scale bars, 50 μm.

clusters were AR-negative, consistent with their NEPC derivation (**Fig. 4E**). qRT-PCR using human-specific GAPDH revealed that the percentages of LuCaP 49 cells in the lungs of batiraxcept monotherapy–treated mice were <5% of vehicle controls, whereas human LuCaP 49 cells in carboplatin-treated mice were reduced only 33% compared with the controls (**Fig. 4F**). The combination of batiraxcept and carboplatin further decreased the spreading of LuCaP 49 metastatic cells in the lungs compared with single-agent treatments (**Fig. 4F**). Therefore, batiraxcept alone or in combination with carboplatin can strongly suppress NEPC growth in the bone and suppress metastasis to the lungs.

Batiraxcept suppresses cancer stemness in CRPC

To understand the mechanisms by which AXL inhibition suppressed mPCa AC in the bone microenvironment, we profiled the transcriptomes of LuCaP 147 and 147CR intratibial tumors with or without batiraxcept treatment by RNA-seq. LuCaP 147CR tumors showed high mRNA levels of GAS6 and AXL as well as known downstream targets of the AXL signaling pathway, including AKT (PIK3CB, PIK3AP1, and PIK3R5), JAK (JAK1), and MAPK (MAP3K13). Interestingly, transcript levels of genes associated with cancer stemness (*CD44*, *TACSTD2, ATXN1*, and *ALDH1A1*) were higher in 147CR tumors compared with 147 tumors (**Fig. 5A**), consistent with previous findings that stemness plays a role in castration-resistance (18). Single-agent batiraxcept treatment significantly reduced the expressions of GAS6, PIK3R5, JAK1, CD44, TACSTD2, and ATXN1 in LuCaP 147CR tumors compared with vehicle-treated tumors, suggesting that AXL inhibition suppressed stemness in these tumors. In contrast, no significant differences in mRNA expression of *GAS6*, *AXL*, *PIK3CB*, *PIK3AP1*, *PIK3R5*, *JAK1*, *MAP3K13*, *CD44*, *TACSTD2*, or *ATXN1* were observed in docetaxel-treated tumors compared with vehicle-treated controls

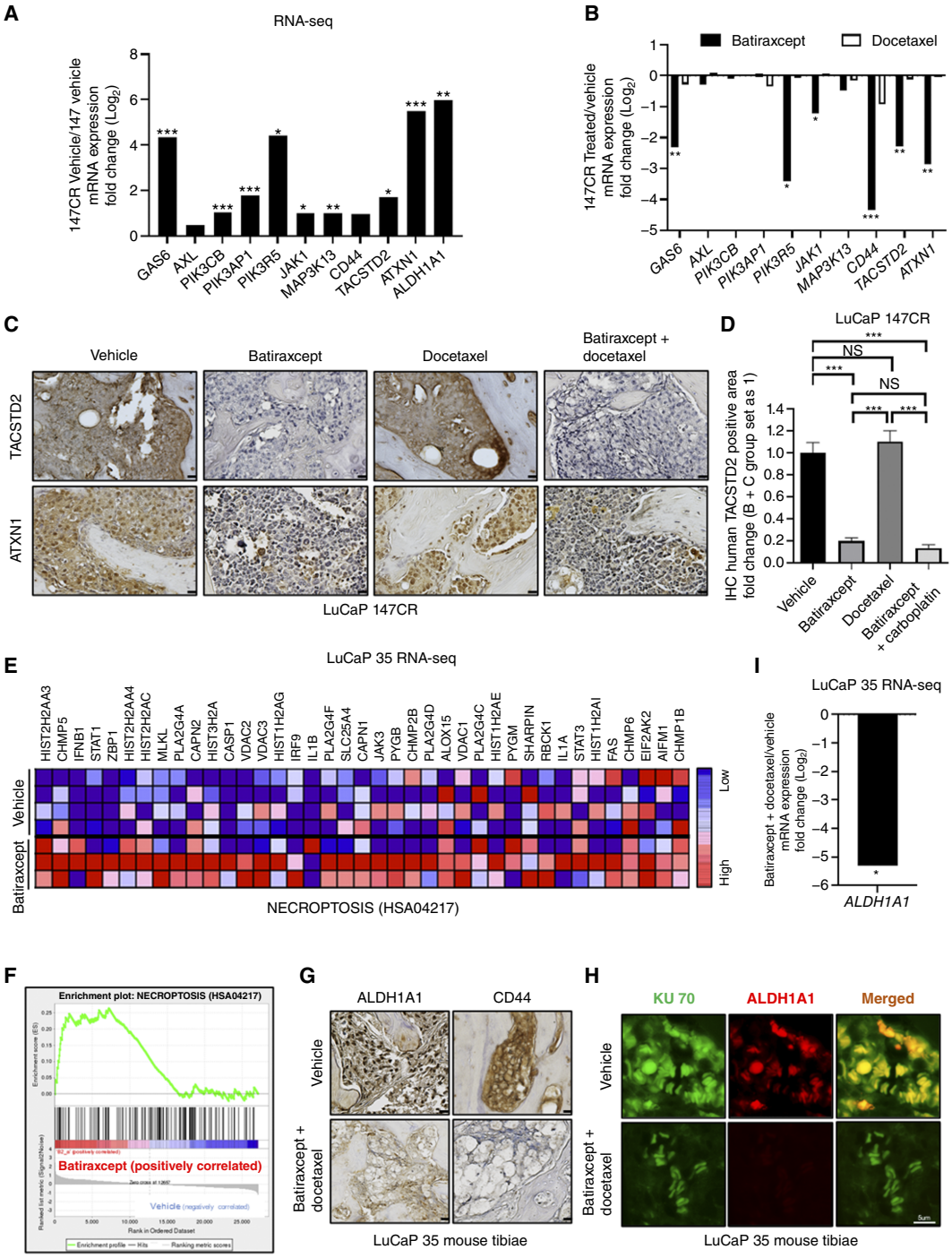

Figure 5.

The mechanisms of action of batiraxcept in CRPC cells. **A,** LuCaP 147CR PDX intratibial tumors expressed higher mRNA of *AXL* (*GAS6*, *AXL*), *AKT* (*PIK3CB*, *PIK3AP1*, and *PIK3R5*), *JAK* (*JAK1*), and *MAPK* (*MAP3K13*) signaling and cancer stemness-associated genes (*CD44*, *TACSTD2*, *ATXN1*, and *ALDH1A1*) compared with parental LuCaP 147 tumors. **B,** Batiraxcept treatment significantly inhibited mRNA expressions of *GAS6, PIK3R5, CD44, TACSTD2*, and *ATXN1* genes in LuCaP 147CR PDX intratibial tumors compared with the vehicle-treated controls. **C** and **D,** Representative images (**C**) and quantification of IHC staining of TACSTD2 (**D**) and ATXN1 antibodies on intratibial LuCaP 147CR PDX tumors in vehicle, batiraxcept, docetaxel, and combination therapy groups. **E,** Heatmap shows the relative expression of necroptosis (HSA04217) genes between batiraxcept monotherapy and vehicle controls. **F,** GSEA demonstrating that batiraxcept treatment correlated with necroptosis in intratibial LuCaP 35 PDX tumors. **G,** Combination therapy of batiraxcept and docetaxel inhibited the expression of ALDH1A1 and CD44 proteins in LuCaP 35 PDX bone tumors. **H,** Representative immunofluorescence images of Ku70 and ALDH1A1 showed fewer ALDH1A1-positive stem-like cells with combination therapy compared with controls. **I,** Intratibial LuCaP 35 tumors treated with combination therapy show significant downregulation of *ALDH1A1* mRNA. *, $P < 0.05$; **, $P < 0.01$; ***, $P < 0.001$; NS, $P > 0.05$ not significant. All scale bars, 10 μm.

(**Fig. 5B**). Consistently, TACSTD2 and ATXN1 protein levels were significantly reduced in batiraxcept-treated tumors as a single agent or in combination with docetaxel compared with controls, as determined by IHC (**Fig. 5C**), whereas no changes in TACSTD2 protein levels were observed in docetaxel-treated tumors compared with controls (**Fig. 5D**). In LuCaP 35 tumors, RNA-seq revealed that batiraxcept as a single agent induced the expression of necroptosis-associated genes such as *HIST2H2AA3*, *CHMP5*, *IFNB1*, *STAT1*, and *ZBP1* (**Fig. 5E**), and GSEA confirmed enrichment of the necroptosis pathway in batiraxcept-treated tumors compared with controls (**Fig. 5F**). Finally, combination therapy of batiraxcept and docetaxel decreased the expression of stemness markers CD44 and ALDH1A1, as evaluated by IHC and immunofluorescence staining (**Fig. 5G** and **H**), which was consistent with the observation of lower ALDH1A1 mRNA levels by RNA-seq in tumors treated with combination therapy compared with controls (**Fig. 5I**). These results suggest that AXL inhibition suppresses tumor growth in the bone microenvironment through multiple mechanisms, including decreasing cancer stemness and induction of necroptosis.

Identification of pathways affected by batiraxcept treatment of prostate cancer cells in the bone microenvironment

To characterize the pathways targeted by the single agent batiraxcept and combination therapy with docetaxel, we performed IHC staining and Western blotting to assess the AXL signaling pathway in intratibial LuCaP 147CR and LuCaP 35 tumors (**Fig. 6A** and **B**; Supplementary Fig S6) compared with controls. Total AXL protein levels were similar in both groups. However, IHC staining for phospho-AXL, indicating activation of AXL signaling, was significantly lower in batiraxcept-treated tumors. Likewise, AKT, immediately downstream of AXL (39–41), showed no change in total protein levels, but phospho-AKT was significantly decreased in batiraxcept-treated tumors compared with controls (**Fig. 6A**; Supplementary Fig S6). Since AXL can also modulate MAPK signaling (39), we evaluated ERK and found that total protein levels of ERK did not change (or increased slightly on Western blot), whereas phospho-ERK decreased significantly after AXL inhibition alone or in combination with docetaxel (**Fig. 6A** and **B**; Supplementary Fig S6). Interestingly, treatment with a single agent of batiraxcept or combination therapy of batiraxcept significantly decreased protein levels of transcription factor E2F1 and its downstream target NUSAP1 (**Fig. 6A** and **B**; ref. 42). Therefore, inhibition of AXL signaling with batiraxcept or batiraxcept combined with docetaxel acts directly to suppress several downstream signaling pathways in the bone microenvironment (**Fig. 6C**). Based on these findings, the combination therapy of batiraxcept and docetaxel or carboplatin could provide a novel therapeutic strategy to treat prostate cancer metastatic to the bone that has failed hormonal therapy (**Fig. 6D**).

Discussion

In bone biopsies from patients with mPCa, we demonstrated that p-AXL expression was associated with poor clinical outcomes. In LuCaP mPCa AC and NEPC PDX implanted intratibially, AXL inhibition by batiraxcept suppressed tumor growth and metastasis to the lungs more effectively than docetaxel or carboplatin in androgen-independent tumors. Moreover, combination therapy with batiraxcept and docetaxel and/or carboplatin was more effective than either alone in inhibiting tumor growth in both CRPC and NEPC. Finally, batiraxcept as a single agent blocked metastasis of intratibial tumors to the lungs more effectively than docetaxel or carboplatin alone. These findings provide a strong rationale for clinical testing of batiraxcept as a single agent or in combination with docetaxel or carboplatin to treat patients with prostate cancer metastatic to the bone (16, 17).

Batiraxcept has demonstrated significant therapeutic effects in preclinical models of multiple cancers (40, 43) and is being evaluated in clinical trials for several cancer types. When combined with paclitaxel, batiraxcept elicited an overall response rate of 34.8% with two complete responses in a phase 1b trial in ovarian cancer (NCT03639246). In a phase III study, the combination did not significantly improve progression-free survival (PFS) compared with paclitaxel alone (NCT04729608). However, in a secondary analysis focusing on patients in whom ovarian cancers expressed high levels of AXL (20% of total patient population), median PFS was 5.78 months in the batiraxcept + paclitaxel arm and 3.71 months in the control paclitaxel arm, HR 0.55 (CI, 0.31–0.98; $P = 0.042$), and median OS was 17.8 months in the batiraxcept + paclitaxel cohort and 8.11 months in the paclitaxel cohort, HR 0.32 (CI, 0.14–0.73; $P = 0.006$). Therefore, in patients selected for high tumor expression of AXL, batiraxcept improves both PFS and OS in patients with ovarian cancer with high AXL expression when combined with paclitaxel compared with paclitaxel alone (NCT04729608; ref. 44). In the mCRPC bone metastasis samples examined in our study, 61% expressed high levels of AXL protein. Thus, high tumor AXL levels could be used to identify the subset of patients with CRPC who could benefit from batiraxcept in combination with taxanes. Currently, batiraxcept is being tested in clinical trials of clear cell renal cell carcinoma (NCT04300140), pancreatic cancer (NCT04983407; ref. 10), urothelial carcinoma (NCT04004442), uterine cancer (NCT05826015), and platinum-resistant or recurrent ovarian, fallopian tube, or primary peritoneal cancer (NCT04019288).

Proteomic and transcriptomic analyses of treated prostate cancer PDX tumors revealed several molecular mechanisms through which batiraxcept inhibits mPCa bone tumor growth and metastasis. In LuCaP PCa PDX, batiraxcept inhibited the AKT signaling pathway in other cancer types (40, 41). Interestingly, batiraxcept suppressed cancer stemness genes (*CD44*, *TACSTD2*, *ATXN1*, and *ALDH1A1*) at both transcript and protein levels. AXL is a direct downstream target of YAP/TAZ signaling in the CRPC-SCL subtype identified recently in organoids derived from human tissues (18). Since the CRPC-SCL comprised a significant fraction of CRPC in human datasets, AXL inhibition could be used to target this subtype specifically. In addition, GSEA showed that batiraxcept induces necroptosis in intratibial mPCa PDX tumors, consistent with a previous report in which a necroptosis sensitivity screen in 941 human cancer cell lines identified AXL as a mediator of necroptosis because its inhibition can result in restoring sensitivity to necroptosis (45). The mechanisms of action in batiraxcept were confirmed by IHC and Western blotting, showing that batiraxcept suppressed AXL, AKT, MAPK, E2F1, and NUSAP1 signaling pathways at the protein level, whereas docetaxel treatment did not. Therefore, batiraxcept and docetaxel differentially affect these essential signaling pathways in cancer progression; batiraxcept directly targets stem cell driver pathways in prostate cancer, suppressing growth and metastases, whereas docetaxel does not.

In our PDX models, batiraxcept significantly reduced tumor growth when combined with docetaxel and carboplatin compared with either agent alone. Genetic or pharmacologic inhibition of AXL has been shown to enhance the response of various cancers to taxanes, including mesenchymal, uterine, ovarian, and breast

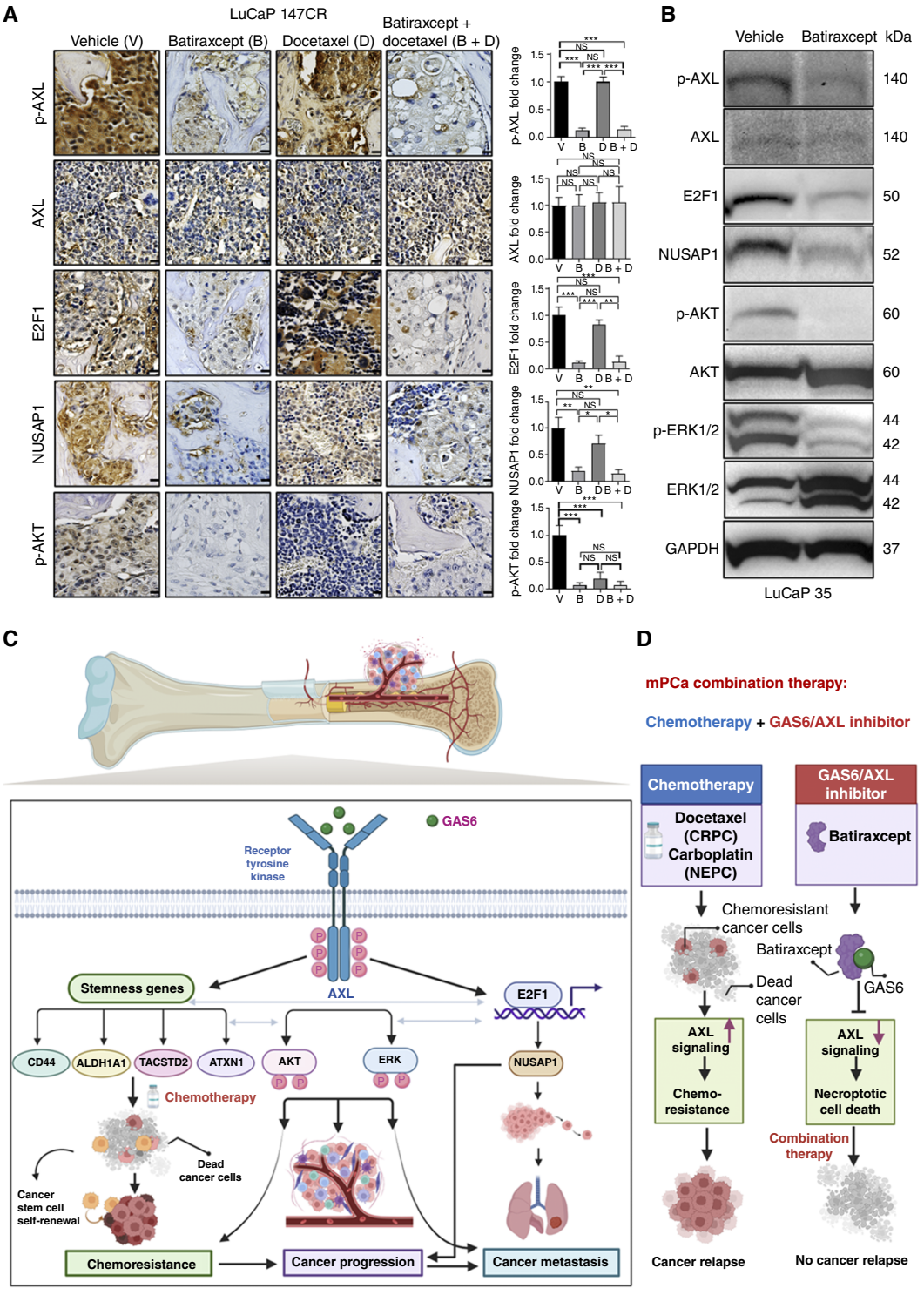

Figure 6.

The molecular mechanisms of batiraxcept in prostate cancer cells in the bone microenvironment. **A,** IHC staining demonstrates batiraxcept alone or in combination with docetaxel reduced p-AXL, E2F1, NUSAP1, and p-AKT protein levels compared with vehicle-treated controls in the intratibial LuCaP 147CR PDX model. Scale bar, 10 μm. **B,** Western blots demonstrated batiraxcept treatment downregulated p-AXL, E2F1, NUSAP1, p-AKT, and p-ERK1/2 in intratibial LuCaP 35 PDX tumors. **C,** Summary of AXL signaling pathways of prostate cancer cells in the bone microenvironment. **D,** Proposed mechanism of action for batiraxcept and docetaxel or carboplatin combination therapy to inhibit tumor growth and metastasis as well as overcome chemoresistance in prostate cancer metastatic to the bone. *, $P < 0.05$; **, $P < 0.01$; ***, $P < 0.001$; NS, $P > 0.05$ not significant. (**C** and **D,** Created with BioRender. Chiu, C. [2025], https://BioRender.com/f51l010, https://BioRender.com/w94d739, and https://BioRender.com/g56q608.)

(46, 47), and to platinum-based drugs (48, 49), likely through the inhibition of PI3K/AKT, MAPK/ERK, NF-κB, and c-ABL signaling (39, 50, 51). In the presence of GAS6, the viability of prostate cancer cells treated with docetaxel is significantly increased (16), and forced AXL overexpression in prostate cancer cells is sufficient to induce resistance to docetaxel (14). Moreover, inhibition of AXL suppressed the growth of docetaxel-resistant prostate cancer cell line–derived subcutaneous xenografts, and these effects were significantly augmented when AXL inhibition was combined with docetaxel treatment (14). In addition to the molecular mechanisms employed by batiraxcept to inhibit mPCa progression that we identified, the treatment effects may be explained by a recent report that GAS6 secreted by osteoblasts as well as prostate cancer cells is present at high levels in the bone microenvironment, thereby activating the AXL signaling pathway specifically in prostate cancer bone metastases (16, 19, 20), which in turn induces dormancy of prostate cancer cells in the bone and protects them from therapies targeting proliferation such as docetaxel.

Broadly speaking, the addition of targeted therapies to docetaxel regimens has failed to significantly improve outcomes for patients with mCRPC (52). Although several tyrosine kinase inhibitors that block AXL have been tested in mCRPC and NEPC, including dasatinib, axitinib, tivozanib, crizotinib and cabozantinib, none of these TKIs have shown improvements in survival, either alone or in combination with docetaxel. The best studied of these, cabozantinib, is a potent inhibitor of VEGFR, MET, and several tyrosine kinases including AXL (53). Cabozantinib failed to improve OS in COMET-1, a phase III prospective randomized trial of heavily treated men with mCRPC (54). However, these results must be placed in context before dismissing consideration of batiraxcept as a candidate therapy. Compared with cabozantinib and other TKIs, batiraxcept inhibits AXL signaling with high specificity at clinically achievable dosing. In cell-based assays, cabozantinib inhibited phosphorylation of AXL at relatively high dosage levels (IC_{50}: 42 μmol/L; refs. 53, 55), whereas batiraxcept suppresses serum GAS6 (the ligand for AXL) to levels below the limits of detection by a validated ELISA in healthy volunteers at a dose of only 1 mg/kg (56). Therefore, batiraxcept eliminates AXL signaling with high specificity and without toxicity because AXL is not required for normal tissue function (57). On the other hand, cabozantinib given at doses necessary to achieve clinical responses shows significant toxicity, particularly hepatotoxicity, because of the important roles of VEGFR2 and MET in normal development and tissue repair (58, 59).

While COMET-1 did not demonstrate improvement in OS, a pooled analysis of 1147 patients with mCRPC from COMET-1 and COMET-2 trials demonstrated improved OS (HR 0.80, 95% CI, 0.67–0.95; $P = 0.012$) for cabozantinib after adjusting for other prognostic factors (60). In a recent phase II study comparing cabozantinib plus docetaxel/prednisone versus docetaxel/prednisone alone, the median time to progression and OS time favored the addition of cabozantinib (21.0 vs. 6.6 months; $P = 0.035$ and 23.8 vs. 15.6 months; $P = 0.072$, respectively; ref. 61). Analysis of secondary endpoints in COMET-1 demonstrated that cabozantinib significantly improved radiographic PFS (median 5.6 vs. 2.8 months; $P < 0.001$; ref. 54). In the COMET-2 trial, there was a trend for better OS (9 vs. 7.9 months; HR 0.71, 95% CI, 0.45–1.12; $P = 0.121$) and significantly higher bone scan response with cabozantinib (31% vs. 5.2%; $P < 0.001$; ref. 62). Moreover, in a phase II nonrandomized expansion study of pretreated mCRPC patients with bone metastases, cabozantinib improved bone scans, pain scores, analgesic use, measurable soft tissue disease, circulating tumor cells, and bone biomarkers (63, 64). A recent phase II trial of treatment-naive mCRPC patients with bone metastases showed that cabozantinib induced significant improvements on bone scans in one-third of patients with higher BMP–2 levels at baseline (65). Since one-third of CRPC have been characterized as SCL and driven by AXL expression (18), it is possible that these cancers account for bone scan responses seen with AXL inhibition. In ovarian and kidney cancers, high serum sAXL/GAS6 ratios are associated with improved overall response rates, suggesting that proper patient selection could be used to identify patients likely to benefit from batiraxcept (41, 66, 67). Given the absence of side effects at the highest doses of batiraxcept administered in a Phase I clinical trial (NCT03401528) and the effectiveness of batiraxcept across diverse prostate cancer bone PDXs, clinical testing of batiraxcept could be warranted, particularly in tumors displaying high AXL pathway activity.

Over the past several years, treatment of advanced prostate cancer has shifted toward intensive therapy for metastatic hormone–sensitive prostate cancer, including dual inhibition of androgen signaling, docetaxel, and radiation therapy (68). While these approaches have significantly improved survival, nearly all patients have shown progression. While it is unknown whether AXL inhibition is effective in castration-sensitive prostate cancer, batiraxcept demonstrated significant activity in prostate cancer models derived from heavily treated mCRPC similar to these patients. Given the limited treatment options for these patients, clinical testing of batiraxcept in these patients could be warranted.

In conclusion, batiraxcept as a single agent or in combination with docetaxel or carboplatin significantly reduces prostate cancer growth in the bone microenvironment and inhibits metastasis through multiple mechanisms of action. Therefore, tackling lethal mPCa in the bone microenvironment by batiraxcept, particularly in combination therapy with docetaxel or carboplatin, can potentially overcome chemoresistance and target intractable cancer stem cells in the bone marrow niche. These results nominate batiraxcept as a novel candidate for AXL-targeting therapy for patients with mCRPC or NEPC that is metastatic to the bone.

Authors' Disclosures

C.-L. Chiu reports grants from US Department of Defense and nonfinancial support from Aravive, Inc., during the conduct of the study. M.T. Thomsen reports grants from the Novo Nordisk Foundation outside the submitted work. R.M. Wen reports grants from the US Department of Defense during the conduct of the study. E. Corey reports grants from NIH and other support from Institute for Prostate Cancer Research during the conduct of the study, as well as other support from AbbVie, Gilead Sciences, Sanofi, Zenith Epigenetics, Bayer Pharmaceuticals, Forma Therapeutics, Genentech, GSK, Janssen Research, Kronos Bio, Foghorn Therapeutics, K36 Therapeutics, and MacroGenics and personal fees from Dotquant outside the submitted work. Y.R. Miao reports nonfinancial support from Akso Biopharmaceutical Inc. outside the submitted work. E.B. Rankin reports a patent for PCT/US2013/07478 issued and with royalties paid. J. Huang reports personal fees from Sisu Pharma, Chimigen Bio, York Biotechnology, OptraSCAN, MORE Health, Inc., KingMed Diagnostics, and Artera outside the submitted work. J.D. Brooks reports grants from NIH and nonfinancial support from Aravive, Inc., during the conduct of the study. No disclosures were reported by the other authors.

Authors' Contributions

C.-L. Chiu: Conceptualization, formal analysis, investigation, visualization, methodology, writing–original draft. **D. Zhang:** Formal analysis, investigation, writing–review and editing. **H. Zhao:** Conceptualization, formal analysis, investigation, methodology, writing–review and editing. **Y. Wei:** Investigation. **A.L. Polasko:** Investigation, writing–review and editing. **M.T. Thomsen:** Investigation, writing–review and editing. **V. Yang:** Investigation. **K.K. Yang:** Investigation.

S. Hauck: Investigation. **E.E. Peterson:** Investigation. **R.M. Wen:** Investigation, writing–review and editing. **Z. Qiu:** Investigation. **E. Corey:** Resources, writing–review and editing. **Y.R. Miao:** Resources. **E.B. Rankin:** Resources. **D.M. Peehl:** Resources, methodology, writing–review and editing. **J. Huang:** Resources. **A.J. Giaccia:** Resources. **J.D. Brooks:** Conceptualization, resources, formal analysis, supervision, funding acquisition, methodology, writing–review and editing.

Acknowledgments

Batiraxcept (AVB-S6-500) was kindly provided by Aravive, Inc. This work was supported by the US Department of Defense Postdoctoral and Clinical Fellowship Award (W81XWH2210651 to C.-L. Chiu) and NIH, NCI grants U01, R21, and RO1 (U01 CA196387 and R21 CA245595 to J.D. Brooks; RO1 CA272432 to E.B. Rankin). This research was supported by a Stand Up To Cancer–Prostate Cancer Foundation Prostate Cancer Dream Team Award, grant number SU2C-AACR-DT0812 (PI: E.J. Small). Stand Up To Cancer is a division of the Entertainment Industry Foundation. This research grant was administered by the American Association for Cancer Research, the scientific partner of SU2C. R.M. Wen was supported by the DoD Young Investigator Award (W81XWH2110195). We thank Dr. Eric J. Small and William S. Chen for sharing samples and helpful discussions and Chiyuan Amy Zhang for helpful advice on biostatistics.

Note

Supplementary data for this article are available at Clinical Cancer Research Online (http://clincancerres.aacrjournals.org/).

Received September 19, 2024; revised November 22, 2024; accepted January 27, 2025; published first January 29, 2025.

References

1. Siegel RL, Giaquinto AN, Jemal A. Cancer statistics, 2024. CA Cancer J Clin 2024;74:12–49.
2. Shou J., Zhang Q, Wang S, Zhang D. The prognosis of different distant metastases pattern in prostate cancer: a population based retrospective study. Prostate 2018;78:491–7.
3. Coleman RE. Clinical features of metastatic bone disease and risk of skeletal morbidity. Clin Cancer Res 2006;12:6243s–9.
4. Nevedomskaya E, Baumgart SJ, Haendler B. Recent advances in prostate cancer treatment and drug discovery. Int J Mol Sci 2018;19:1359.
5. Hussain M, Tangen CM, Berry DL, Higano CS, Crawford ED, Liu G, et al. Intermittent versus continuous androgen deprivation in prostate cancer. N Engl J Med 2013;368:1314–25.
6. Lowrance WT, Roth BJ, Kirkby E, Murad MH, Cookson MS. Castration-resistant prostate cancer: AUA guideline Amendment 2015. J Urol 2016;195:1444–52.
7. Chen WS, Aggarwal R, Zhang L, Zhao SG, Thomas GV, Beer TM, et al. Genomic drivers of poor prognosis and enzalutamide resistance in metastatic castration-resistant prostate cancer. Eur Urol 2019;76:562–71.
8. Armstrong CM, Gao AC. Drug resistance in castration resistant prostate cancer: resistance mechanisms and emerging treatment strategies. Am J Clin Exp Urol 2015;3:64–76.
9. He Y, Xu W, Xiao YT, Huang H, Gu D, Ren S. Targeting signaling pathways in prostate cancer: mechanisms and clinical trials. Signal Transduct Target Ther 2022;7:198.
10. Miao YR, Rankin EB, Giaccia AJ. Therapeutic targeting of the functionally elusive TAM receptor family. Nat Rev Drug Discov 2024;23:201–17.
11. Paccez JD, Vasques GJ, Correa RG, Vasconcellos JF, Duncan K, Gu X, et al. The receptor tyrosine kinase Axl is an essential regulator of prostate cancer proliferation and tumor growth and represents a new therapeutic target. Oncogene 2013;32:689–98.
12. Vanli N, Sheng J, Li S, Xu Z, Hu GF. Ribonuclease 4 is associated with aggressiveness and progression of prostate cancer. Commun Biol 2022;5:625.
13. Tanaka M, Dykes SS, Siemann DW. Inhibition of the Axl pathway impairs breast and prostate cancer metastasis to the bones and bone remodeling. Clin Exp Metastasis 2021;38:321–35.
14. Lin JZ, Wang ZJ, De W, Zheng M, Xu WZ, Wu HF, et al. Targeting AXL overcomes resistance to docetaxel therapy in advanced prostate cancer. Oncotarget 2017;8:41064–77.
15. Brown NE, Jones A, Hunt BG, Waltz SE. Prostate tumor RON receptor signaling mediates macrophage recruitment to drive androgen deprivation therapy resistance through Gas6-mediated Axl and RON signaling. Prostate 2022;82:1422–37.
16. Shiozawa Y, Pedersen EA, Patel LR, Ziegler AM, Havens AM, Jung Y, et al. GAS6/AXL axis regulates prostate cancer invasion, proliferation, and survival in the bone marrow niche. Neoplasia 2010;12:116–27.
17. Axelrod HD, Valkenburg KC, Amend SR, Hicks JL, Parsana P, Torga G, et al. AXL is a putative tumor suppressor and dormancy regulator in prostate cancer. Mol Cancer Res 2019;17:356–69.
18. Tang F, Xu D, Wang S, Wong CK, Martinez-Fundichely A, Lee CJ, et al. Chromatin profiles classify castration-resistant prostate cancers suggesting therapeutic targets. Science 2022;376:eabe1505.
19. Mishra A, Wang J, Shiozawa Y, McGee S, Kim J, Jung Y, et al. Hypoxia stabilizes GAS6/Axl signaling in metastatic prostate cancer. Mol Cancer Res 2012;10:703–12.
20. Jung Y, Decker AM, Wang J, Lee E, Kana LA, Yumoto K, et al. Endogenous GAS6 and Mer receptor signaling regulate prostate cancer stem cells in bone marrow. Oncotarget 2016;7:25698–711.
21. Lee CH, Decker AM, Cackowski FC, Taichman RS. Bone microenvironment signaling of cancer stem cells as a therapeutic target in metastatic prostate cancer. Cell Biol Toxicol 2020;36:115–30.
22. Kariolis MS, Miao YR, Jones DS 2nd, Kapur S, Mathews II, Giaccia AJ, et al. An engineered Axl 'decoy receptor' effectively silences the Gas6-Axl signaling axis. Nat Chem Biol 2014;10:977–83.
23. Saar M, Zhao H, Nolley R, Young SR, Coleman I, Nelson PS, et al. Spheroid culture of LuCaP 147 as an authentic preclinical model of prostate cancer subtype with SPOP mutation and hypermutator phenotype. Cancer Lett 2014;351:272–80.
24. Wen RM, Qiu Z, Marti GEW, Peterson EE, Marques FJG, Bermudez A, et al. AZGP1 deficiency promotes angiogenesis in prostate cancer. J Transl Med 2024;22:383.
25. Valta MP, Zhao H, Saar M, Tuomela J, Nolley R, Linxweiler J, et al. Spheroid culture of LuCaP 136 patient-derived xenograft enables versatile preclinical models of prostate cancer. Clin Exp Metastasis 2016;33:325–37.
26. Quigley DA, Dang HX, Zhao SG, Lloyd P, Aggarwal R, Alumkal JJ, et al. Genomic hallmarks and structural variation in metastatic prostate cancer. Cell 2018;174:758–69.e9.
27. Takabatake K, Tsujigiwa H, Song Y, Matsuda H, Kawai H, Fujii M, et al. The role of bone marrow-derived cells during ectopic bone formation of mouse femoral muscle in GFP mouse bone marrow transplantation model. Int J Med Sci 2018;15:748–57.
28. Kim J, Nam G, Shin YK, Vilaplana-Lopera N, Jeung HC, Moon EJ, et al. Targeting AXL using the AVB-500 soluble receptor and through genetic knockdown inhibits bile duct cancer growth and metastasis. Cancers (Basel) 2023;15:1882.
29. Chen CH, Chiu CL, Adler KB, Wu R. A novel predictor of cancer malignancy: up-regulation of myristoylated alanine-rich C kinase substrate phosphorylation in lung cancer. Am J Respir Crit Care Med 2014;189:1002–4.
30. Chen CH, Statt S, Chiu CL, Thai P, Arif M, Adler KB, et al. Targeting myristoylated alanine-rich C kinase substrate phosphorylation site domain in lung cancer. Mechanisms and therapeutic implications. Am J Respir Crit Care Med 2014;190:1127–38.
31. Nguyen HM, Vessella RL, Morrissey C, Brown LG, Coleman IM, Higano CS, et al. LuCaP prostate cancer patient-derived xenografts reflect the molecular heterogeneity of advanced disease and serve as models for evaluating cancer therapeutics. Prostate 2017;77:654–71.
32. Hasegawa T, Someya M, Hori M, Matsumoto Y, Nakata K, Nojima M, et al. Expression of Ku70 predicts results of radiotherapy in prostate cancer. Strahlenther Onkol 2017;193:29–37.
33. Hasegawa T, Someya M, Hori M, Tsuchiya T, Fukushima Y, Matsumoto Y, et al. Prediction of results of radiotherapy with Ku70 expression and an artificial neural network. In Vivo 2020;34:2865–72.
34. Wu ZY, Chiu CL, Lo E, Lee YRJ, Yamada S, Lo SH. Hyperactivity of Mek in TNS1 knockouts leads to potential treatments for cystic kidney diseases. Cell Death Dis 2019;10:871.
35. Chiu CL, Li CG, Verschueren E, Wen RM, Zhang D, Gordon CA, et al. NUSAP1 binds ILF2 to modulate R-loop accumulation and DNA damage in prostate cancer. Int J Mol Sci 2023;24:6258.

36. Gordon CA, Gong X, Ganesh D, Brooks JD. NUSAP1 promotes invasion and metastasis of prostate cancer. Oncotarget 2017;8:29935–50.
37. Heczey A, Xu X, Courtney AN, Tian G, Barragan GA, Guo L, et al. Anti-GD2 CAR-NKT cells in relapsed or refractory neuroblastoma: updated phase 1 trial interim results. Nat Med 2023;29:1379–88.
38. Taichman RS, Patel LR, Bedenis R, Wang J, Weidner S, Schumann T, et al. GAS6 receptor status is associated with dormancy and bone metastatic tumor formation. PLoS One 2013;8:e61873.
39. Rankin EB, Giaccia AJ. The receptor tyrosine kinase AXL in cancer progression. Cancers (Basel) 2016;8:103.
40. Toboni MD, Lomonosova E, Bruce SF, Tankou JI, Mullen MM, Schab A, et al. Inhibition of AXL and VEGF-A has improved therapeutic efficacy in uterine serous cancer. Cancers (Basel) 2021;13:5877.
41. Bruce SF, Cho K, Noia H, Lomonosova E, Stock EC, Oplt A, et al. GAS6-AXL inhibition by AVB-500 overcomes resistance to paclitaxel in endometrial cancer by decreasing tumor cell glycolysis. Mol Cancer Ther 2022;21:1348–59.
42. Gulzar ZG, McKenney JK, Brooks JD. Increased expression of NuSAP in recurrent prostate cancer is mediated by E2F1. Oncogene 2013;32:70–7.
43. Xiao Y, Zhao H, Tian L, Nolley R, Diep AN, Ernst A, et al. S100A10 is a critical mediator of GAS6/AXL-induced angiogenesis in renal cell carcinoma. Cancer Res 2019;79:5758–68.
44. Fuh KC, Tsitsishvili Z, Reid TJ, De Giorgi U, Hand L, Bowen R, et al. AXL-erate-OC/GOG-3059/ENGOT OV-66: results of a phase 3, randomized, double-blind, placebo/paclitaxel-controlled study of batiraxcept (AVB-S6-500) in combination with paclitaxel in patients with platinum-resistant recurrent ovarian cancer. J Clin Oncol 2024;42(Suppl 17):LBA5515.
45. Najafov A, Zervantonakis IK, Mookhtiar AK, Greninger P, March RJ, Egan RK, et al. BRAF and AXL oncogenes drive RIPK3 expression loss in cancer. PLoS Biol 2018;16:e2005756.
46. Wilson C, Ye X, Pham T, Lin E, Chan S, McNamara E, et al. AXL inhibition sensitizes mesenchymal cancer cells to antimitotic drugs. Cancer Res 2014;74:5878–90.
47. Palisoul ML, Quinn JM, Schepers E, Hagemann IS, Guo L, Reger K, et al. Inhibition of the receptor tyrosine kinase AXL restores paclitaxel chemosensitivity in uterine serous cancer. Mol Cancer Ther 2017;16:2881–91.
48. Hong J, Peng D, Chen Z, Sehdev V, Belkhiri A. ABL regulation by AXL promotes cisplatin resistance in esophageal cancer. Cancer Res 2013;73:331–40.
49. Quinn JM, Greenwade MM, Palisoul ML, Opara G, Massad K, Guo L, et al. Therapeutic inhibition of the receptor tyrosine kinase AXL improves sensitivity to platinum and taxane in ovarian cancer. Mol Cancer Ther 2019;18:389–98.
50. Schoumacher M, Burbridge M. Key roles of AXL and MER receptor tyrosine kinases in resistance to multiple anticancer therapies. Curr Oncol Rep 2017;19:19.
51. Scaltriti M, Elkabets M, Baselga J. Molecular pathways: AXL, a membrane receptor mediator of resistance to therapy. Clin Cancer Res 2016;22:1313–7.
52. Corn P.G, Agarwal N, Araujo JC, Sonpavde G. Taxane-based combination therapies for metastatic prostate cancer. Eur Urol Focus 2019;5:369–80.
53. Yakes FM, Chen J, Tan J, Yamaguchi K, Shi Y, Yu P, et al. Cabozantinib (XL184), a novel MET and VEGFR2 inhibitor, simultaneously suppresses metastasis, angiogenesis, and tumor growth. Mol Cancer Ther 2011;10:2298–308.
54. Smith M, De Bono J, Sternberg C, Le Moulec S, Oudard S, De Giorgi U, et al. Phase III study of cabozantinib in previously treated metastatic castration-resistant prostate cancer: COMET-1. J Clin Oncol 2016;34:3005–13.
55. Zhang Y, Guessous F, Kofman A, Schiff D, Abounader R. XL-184, a MET, VEGFR-2 and RET kinase inhibitor for the treatment of thyroid cancer, glioblastoma multiforme and NSCLC. IDrugs 2010;13:112–21.
56. Bonifacio L, Dodds M, Prohaska D, Moss A, Giaccia A, Tabibiazar R, et al. Target-mediated drug disposition pharmacokinetic/pharmacodynamic model-informed dose selection for the first-in-human study of AVB-S6-500. Clin Transl Sci 2020;13:204–11.
57. Lu Q, Gore M, Zhang Q, Camenisch T, Boast S, Casagranda F, et al. Tyro-3 family receptors are essential regulators of mammalian spermatogenesis. Nature 1999;398:723–8.
58. Wang X, Bove AM, Simone G, Ma B. Molecular bases of VEGFR-2-mediated physiological function and pathological role. Front Cell Dev Biol 2020;8:599281.
59. Kato T. Biological roles of hepatocyte growth factor-Met signaling from genetically modified animals. Biomed Rep 2017;7:495–503.
60. Sonpavde GP, Pond GR, Fizazi K, de Bono JS, Basch EM, Scher HI, et al. Cabozantinib for progressive metastatic castration-resistant prostate cancer following docetaxel: combined analysis of two phase 3 trials. Eur Urol Oncol 2020;3:540–3.
61. Madan RA, Karzai FH, Al Harthy M, Petrylak DP, Kim JW, Arlen PM, et al. Cabozantinib plus docetaxel and prednisone in metastatic castration-resistant prostate cancer. BJU Int 2021;127:435–44.
62. Basch EM, Scholz MC, De Bono JS, Vogelzang NJ, De Souza PL, Marx GM, et al. Final analysis of COMET-2: cabozantinib (Cabo) versus mitoxantrone/prednisone (MP) in metastatic castration-resistant prostate cancer (mCRPC) patients (pts) with moderate to severe pain who were previously treated with docetaxel (D) and abiraterone (A) and/or enzalutamide (E). J Clin Oncol 2015;33(Suppl 7):141.
63. Smith DC, Smith MR, Sweeney C, Elfiky AA, Logothetis C, Corn PG, et al. Cabozantinib in patients with advanced prostate cancer: results of a phase II randomized discontinuation trial. J Clin Oncol 2013;31:412–9.
64. Smith MR, Sweeney CJ, Corn PG, Rathkopf DE, Smith DC, Hussain M, et al. Cabozantinib in chemotherapy-pretreated metastatic castration-resistant prostate cancer: results of a phase II nonrandomized expansion study. J Clin Oncol 2014;32:3391–9.
65. Smith DC, Daignault-Newton S, Grivas P, Reichert ZR, Hussain M, Cooney KA, et al. Efficacy and effect of cabozantinib on bone metastases in treatment-naive castration-resistant prostate cancer. Clin Genitourin Cancer 2020;18:332–9 e2.
66. Shah NJ, Campbell MT, Mao SS, Ornstein MC, Haas NB, Gao X, et al. A phase 1b/2 study of batiraxcept (AVB-S6-500) in combination with cabozantinib in patients with advanced or metastatic clear cell renal cell carcinoma (ccRCC). J Clin Oncol 2023;41(Suppl 6):666.
67. Mullen MM, Lomonosova E, Toboni MD, Oplt A, Cybulla E, Blachut B, et al. GAS6/AXL inhibition enhances ovarian cancer sensitivity to chemotherapy and PARP inhibition through increased DNA damage and enhanced replication stress. Mol Cancer Res 2022;20:265–79.
68. Kwon WA, Song Y.S, Lee M.K. Strategic advances in combination therapy for metastatic castration-sensitive prostate cancer: current insights and future perspectives. Cancers (Basel) 2024;16:3187.